Exploration and Visualisation of Full-Waveform LiDAR Data for Forest Monitoring

submitted by

Milto Miltiadou

for the degree of Doctor of Engineering

of the

University of Bath

Centre for Digital Entertainment
Computer Science

November 2016

Abstract

hello world - no more than 300 words We can change colors for emphasis, but who is going pay for the ink?

To be added on top

Abstract

This study focuses on enhancing the visualisations and classifications of forested areas using coincident full-waveform (fw) LiDAR data and hyperspectral images. The ultimate aim is use both datasets to derive information about forests and show the results on a 3D virtual, interactive environment. Influenced by Persson et al (2005), voxelisation is an integral part of this research. The intensity profile of each full-waveform pulse is accumulated into a voxel array, building up a 3D density volume. The correlation between multiple pulses into a voxel representation produces a more accurate representation, which confers greater noise resistance and it further opens up possibilities of vertical interpretation of the data. The 3D density volume is then aligned with the hyperspectral images using a 2D grid similar to Warren et al (2014) and both datasets are used in visualisations and classifications.

Previous work in visualising fw LiDAR has used transparent objects and point clouds, while the output of this system is a coloured 3D-polygon representation, showing well-separated structures such as individual trees and greenhouses. The 3D density volume, generated from the fw LiDAR data, is polygonised using functional representation of object (FReps) and the marching cubes algorithm (Pasko and Savchenko, 1994) (Lorensen and Cline, 1987). Further, an optimisation algorithm is introduced that uses integral volumes (Crow, 1984) to speed up the process of polygonising the volume. This optimisation approach not only works on non-manifold object, but also a speed up of up to `51%` was achieved. The polygon representation is also textured by projecting the hyperspectral images into the mesh. In addition, the output is suitable for direct rendering with commodity 3D-accelerated hardware, allowing smooth visualisation.

In future work, the effects of combining both hyperspectral imagery and fw LiDAR in classifications and visualisations are examined. At first, two pixel wise classifiers, a support vector machine and a Bayesian probabilistic model, will be used for testing the effects of the combination in generating tree coverage maps. Higher accuracy classification results are expected when metrics from both datasets are used together. Regarding the visualisations, the differences of applying surface reconstruction versus direct volumetric rendering will be discussed and an ordered tree structure with integral sums of the node values will be used for speeding up the ray-tracing of direct volumetric rendering and improving memory management of aforementioned optimisation algorithm with integral volumes. Further, deferred rendering is suggested for testing the visual human perception of projecting multiple bands of the hyperspectral images on the FW LiDAR

polygon representations. At the end of this project the combination of the datasets will be used along with the watershed algorithm for tree segmentation, which is useful for measuring the stem density of a forest and for tree species classifications.

from EDE:

Firstly, a new and fast way of aligning the FW LiDAR with Remotely Sensed Images has been developed in DASOS and by generating tree coverage maps it was shown that the combination of those datasets confers better remote survey results. This work was presented at the 36th ISRSE International Conference.

Secondly, automated detection of dead trees in native Australian forests has a significant role in protecting animals, which live in those trees and are close to extinction. DASOS allow the generation of 3D signatures characterising dead trees. A comparison between the discrete and FW LiDAR is performed to demonstrate the increased survey accuracy obtained when the FW LiDAR are used.

Finally, the last application is for improving visualisations for foresters. Foresters have a great knowledge about forests and can derive a wealth of information directly from visualisations of the remotely sensed data. This reduces the travelling time and cost of getting into the forests. This research optimises visualisations by using the new FW LiDAR representations and a speed of up to 51% has been achieved.

FW LiDAR has great potentials in forestry and this research has already started to have an impact in the FW LiDAR community by making those huge datasets easier to handle. DASOS is now used at Interpine Group Ltd, a world leading Forestry Company in New Zealand and it has been tested from a PhD student at Bournemouth University who looks into estimating bird distribution in the New Forest. In the future, it is expected that DASOS will be widely used in remote forest surveys (i.e. estimating the commercial value of a forest and detecting infected trees at early stages for treatment).

Acknowledgements

Above all, I would like to express my great gratitude to my industrial supervisors Dr. Michael Grant who had supported me continuously during my research and gave me the freedom to create a project of my own interest.

Then, I would like to thanks Dr. Matthew Brown, who helped me during my first years of my studies by giving me valuable and informative feedback. He was always there to keep me working on the right track.

Equally important is my current supervisor Dr. Neil D.F. Campbell and he is not to be missed from the acknowledgements.

Furthermore, special thanks are given to Dr. Mark Warren, Dr. Darren Cosker, MSc Susana Gonzalez Aracil and Dr. Ross Hill who occasionally advised me during my studies.

It further worth giving credits to my data providers, the Natural Environment Research Council's Airborne Research and Survey Facility (NERC ARSF) and Interpine Group Ltd.

Last but not least, I am extremely grateful to my funding organisations, the Centre for Digital Entertainement and Plymouth Marine Laboratory, who supported financially and consequently made this research possible.

Abbreviations and Glossary

AGC	Automatic Gain Controller
ALS	Airborne Laser Scanning
APL	Airborne Processing Library
ARSF	Airborne Research and Survey Facility
DASOS	(=forest in Greek), the open source software implemented for managing FW LiDAR data
FW	Full-Waveform
LiDAR	Light Detection And Ranging
NASA	National Aeronautics and Space Administration
NERC	Natural Environment Research Council
VLR	Variable Length Records
WPDF	Waveform Packet Descriptor Format
UK	United Kingdom

Publications

DASOS-User Guide, M. Miltiadou, N.D.F Campbell, M. Brown, S.C. Aracil, M.A. Warren, D. Clewley, D.Cosker, and M. Grant, Full-waveform LiDAR workshop at Interpine Group Ltd, Rotorua NZ, 2016

Alignment of Hyperspectral Imagery and Full-Waveform LiDAR data for visualisation and classification purposes, M. Miltiadou, M. A. Warren, M. Grant, and M. Brown, *The International Archives of Photogrammetry, Remote Sensing and Spatial Information Sciences*, vol. 40, no. 7, p. 1257, 2015.

Reconstruction of a 3D Polygon Representation from Full-Wavefrom LiDAR data, M. Miltiadou, M. Grant, M. Brown, M. Warren, and E. Carolan,*RSPSoc Annual Conference, New Sensors for a Changing World*, 2014.

Awards

EDE and Ravenscroft Prize - Finalist: Selected as one of the five finalists for this is a prestigious prize that recognises the work of best postgraduate researchers.

Student Poster Competition at Silvilaser.

Conference Presentations

ForestSAT Conference, Santiago, Chile, 2016 - Oral and Poster Presentation

Computer Graphics & Visual Computing (CGVC), Bournemouth, United Kingdom, 2016 - Oral Presentation

Silvilaser, La Grant Motte, France, 2015 - Poster Presentation

International Symposium of Remote Sensing of the Environment (ISRSE), 2015 - Oral Presentation

RSPSoc Conference, New Sensors for a Changing world, Aberystwyth, United Kingdom, 2014 - Oral Presentation

Contents

List of Figures

Chapter 1

Introduction

1.1 Forest Monitoring: Importance and Applications

Forest monitoring involves checking and observing the changes in the structure of the forests and their foliage over the years. It has a significant value in both sustainable and commercial forests, because it contributes into managing biodiversity, maintaining forest health and optimising wood trade procedures as explained below:

- **Biodiversity** plays a substantial role in ecosystem resilience [1] while various human activities affect biological communities by altering their composition and leading species to extinction [2]. For example, in Australian native forests many arboreal mammals and birds rely on hollow trees for shelters [3] . Hollow trees are trees that have hollows, which are semi-enclosed cavity on trunks and branches. They are formed by natural forces, like bacteria, fungi and insects and it takes hundreds of years to become suitable for animal/bird shelters. Studies predict shortage of hollows available for colonisation in near future [4] [5]. Therefore monitoring and protecting hollow trees have a positive impact in preserving biodiversity.

- **Forest Health**: Protecting vegetation from pests and diseases. An example of pests are the Brushtail Possums, which were initially brought to New Zealand for fur trade, but they have escaped and become a thread to native forests and vegetation [6]. In addition, anthropogenic factors have a negative impact to nature. For instance, acid rain is responsible for the freezing decease at red bruces because it reduces the membrane-associated calcium, which is important for tolerating cold [7]. Those changes in nature need to be monitor in order to preserve a healthy and resilience ecosystem.

- **Wood Trade**: Measuring stem volume and basal areas of trees contributes to forest planning and management [8]. For example, measuring stocking and wood quality would help into estimating the cost of harvesting the trees in relation to the stocking [9].

Traditionally, forest monitoring involves field work such as travelling into the area of interest and measuring tree diameters and heights. Regarding the need to monitor hollows, tree climbing with ladders and ropes gives very accurate results but it's dangerous, expensive, time consuming, and cannot easily scale into large forested areas [10] [11]. Therefore, automated ways of monitoring forests are essential and this is why Remote Sensing has a significantly positive impact in forestry.

1.2 Background Information about Remote Sensing and Airborne Laser Scanning Systems

Remote sensing refers to the acquisition of information about objects, for example vegetation and archaeological monuments, without physical contact and the interpretation of that information. The sensors used to capture the information are divided into passive and active. For example satellite photography is passive because information are collected from the reflected natural sun light, while Airborne Laser Scanners (ALS) are active because they emit laser beams and collects information from the backscattered laser energy [12].

According to Wanger et al, Airborne Laser Scanning (ALS) is a growing technology used in environmental research to collect information about the earth like vegetation and tree species. Comparing ALS with traditional photography, ALS is not influenced by light and it is therefore less dependant on weather conditions (ie. it collects information from below the clouds). The laser beam further penetrates the tree canopies allowing it to record information about the forest structure below the canopy, as well as the ground [13]. ALS methods are divided into pulse systems, which repeatedly emit pulses, and continuous wavelength systems that continuously emit light. They both acquire information from the backscattered laser intensity over time, but continuous wavelength systems are more complicated because they obtain one extra physical parameter, the frequency of the ranging signal. Further, according to Wehr and Lohr, continuous wavelength systems are 85 times less accurate than pulse systems [14].

LiDAR (Light Detection And Ranging) systems are passive and pulse laser scanning systems [14]. They are divided into two groups according to the diameter of the footprint left by the laser beam on the ground. This diameter depends on the beam divergence and the distance between the sensor and the target. The small-footprint

systems have a 0.2-3m diameter, have been widely commercialised and are mostly carried on planes (ALS systems). In contrast, the large-footprint systems have a wider diameter (10-70m) and during experiments they were mostly adjusted on satellites. Small-footprint systems record at higher resolution but it cannot guarantee that every pulse will reach the ground due to the small diameter of their footprint, making topographic measurements difficult. In contrast, large-footprint scanners have wider diameters and can therefore scan wider areas with the likelihood of recording the ground to be higher [15] .

In addition, there are two types of LiDAR data, the discrete and the full-waveform (FW). The discrete LiDAR records a few peaks of the reflected laser intensity, while the FW LiDAR stores the entire backscattered signal. The discrete LiDAR has been widely used and a 40% reduction of fieldwork has been achieved at Interpine Ltd Group, New Zealand, with that technology. Regarding the FW LiDAR, scientists understand their concepts and potentials but due to the shortage of available tools able to handle these large datasets, there are very few uses of FW LiDAR [16].

The design of the first FW LiDAR system was introduced in 1980s, but the first operational system was developed by NASA in 1999 [17]. The increased amount of information recorded within the FW LiDAR suggests many new possibilities and problems from the point of view of image understanding, remote surveying and visualisation. As an indication, a 9.3GB discrete LiDAR from New Forest, UK, corresponds to 55.7GB of FW LiDAR.

This research is focused on the representations of the FW LiDAR data and contributes in both forestry visualisations and classifications. Two datasets are used for testing and evaluation: the New Forest and the RedGum dataset. An in depth explanation of LiDAR systems and the specifications, differences and challenges of the two dataset are given in and Section 2. An overview of the thesis along with its aims, objectives and contributions are then outlined at Section 3.

Chapter 2

Acquire Data

The Acquire Data section gives a practical and scientific insight about the acquire data, because a good knowledge of these data is essential for understanding the related research undertaken. The relations between the two main datasets used in this project are depicted on Figure 2-1 and briefly explained here:

- The **New Forest dataset** from UK was provided by Natural Environment Research Council's Airborne Research and Survey Facility (NERC ARSF). It was collected using a Leica ALS50-II instrment on the 8th of April in 2010 and contains Discrete LiDAR, FW LiDAR and Hyperpsectral Images.
- The **RedGum dataset** was acquired in Australia using a TRimble AX60 instrument from the 6th of March in 2015 till the 31st of March in 2015 and it was provided by the RPS Australia East Pty Ltd. For this datasets only the FW LiDAR data are used here.

The ALS data are explained first, because they are the main focus of this research and at the end the Hyperspectral Imagery. In Section 2.1, it is given an in depth insight about ALS systems and the differences between discrete and FW LiDAR data. Then at Section 2.2 the binary file format of the acquire LiDAR data is briefly explained and Section 2.3 is a discussion about the limitations, the differences and the advantages of two LiDAR instrument; the Leica and Trimble. By the end, the essential information about the Hyperspectral Imagery, which is only associated with the New Forest dataset, is explained in Section 2.4.

2.1 Airborne LiDAR systems: An in-depth Explanation

The ALS systems emit laser beams from a plane and collects information from the returned laser intensity. When the beam hits an object (i.e. the forest canopy), then

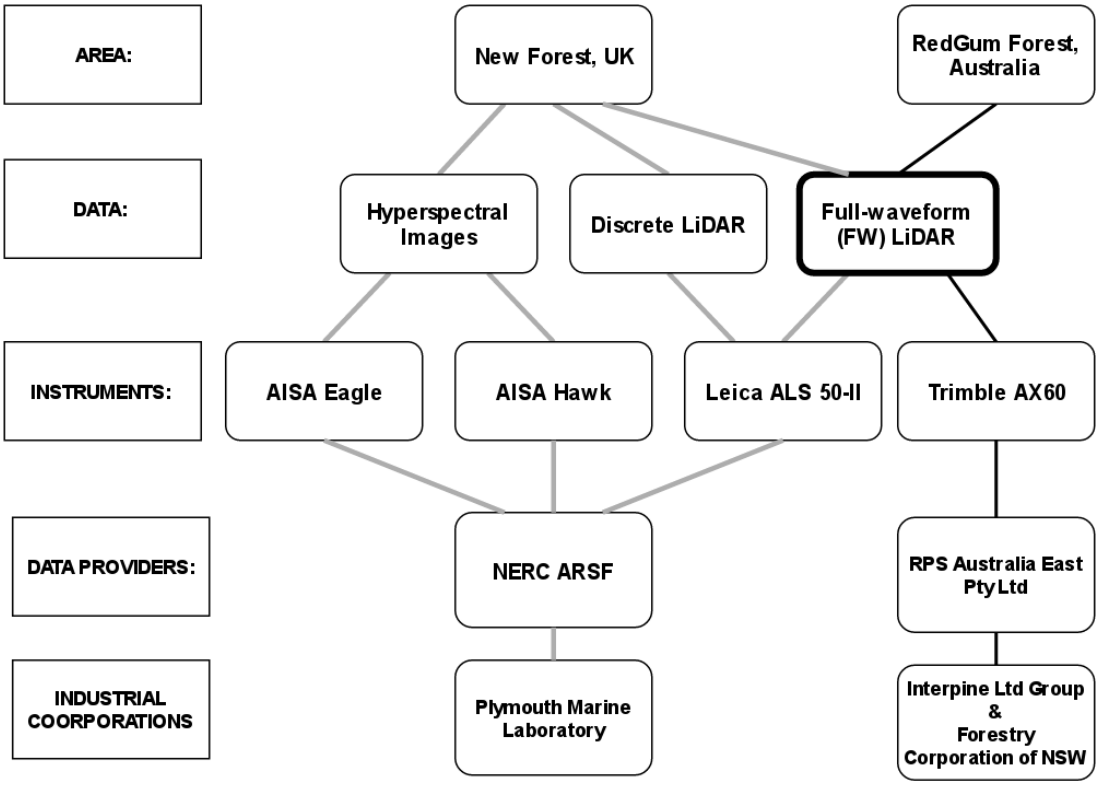

Figure 2-1: Data and Instruments

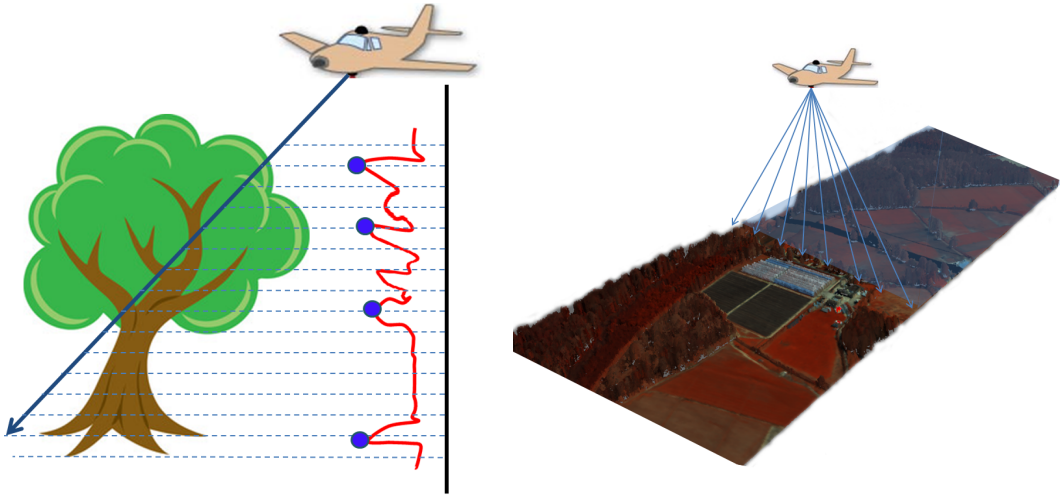

(a) A Pulse: Discrete Vs Full-Waveform (b) A Flightline

Figure 2-2: Airborne Laser Scanning System

some of it bounces back while the rest penetrates through the tree branches. The laser beam continuous to break and partially return to the sensor until it reaches the ground. The LiDAR systems record information from the backscattered laser and by measuring its round trip time.

As mentioned at Section 1.2, there are two types of LiDAR data, the discrete and the FW. The discrete LiDAR records a few peak laser returns, while the FW LiDAR system digitises and records the enitre backscattered signal into equally spaced time intervals (Figure 2-2b). The delivered data for the discrete LiDAR is a set of hit points, returns, which are associated with laser intensities. The position of every return is calculated by measuring the round trip time of the laser beam. The waveforms are attached to first returns of discrete LiDAR data and they are a list of intensities that correspond to the laser intensity returned over time. There is also an offset vector which defines the distance between each wave sample.

Nevertheless, as shown at Figure 2-2a, the scanned data has a limited maximum width according to the flight height and the field of view scan angle. During processing the track of the plane is divided into easier to handle pieces (flightlines) and saved into separate binary files. In this project the LAS1.3 file format is used for both datasets.

2.2 Brief Explanation the LAS1.3 File Format

There are a few LiDAR file formats but the LAS1.3 binary was the first format to contain FW data and it is the one used to store the data for both New Forest and RedGum datasets. According to LAS1.3 file specifications [18], a .LAS file contains information about both discrete and FW LiDAR data and the waveform packets are attached to discrete returns and saved either internally at the end of the .LAS file or externally in a .WVS file.

As shown at (Figure 2-3) the .LAS file is divided into four sections and a brief explanation of each section is given here:

1. The **Header** contains general information about the entire flightline. For example, it includes the scan angle used during the flight, whether the waveform packets are recorded internally or externally and the number of **Variable Length Records** (VLR).

2. Regarding the **VLR**, the most important information given is the waveform packet descriptors that contain essential information on how to read the waveform packets (i.e. an ID, the number of wave samples and the size of each intensity in bits).

3. The **Point Data Records** are the discrete points and the waveforms are associated with first return discrete points. Each Point Data Record has a spatial location, an intensity and optionally a pointer to a waveform packet as well as the ID of the corresponding waveform packet descriptor.

4. The waveform packets is a list of intensities and they are either saved internally into the **Extended Variable Length Records** section of the .LAS file or inside an external .WVS file. Starting from the associated first return point, the spatial location of the waveform packet (wave sample intensity) are calculated by adding an offset defined in the associated Point Data Record.

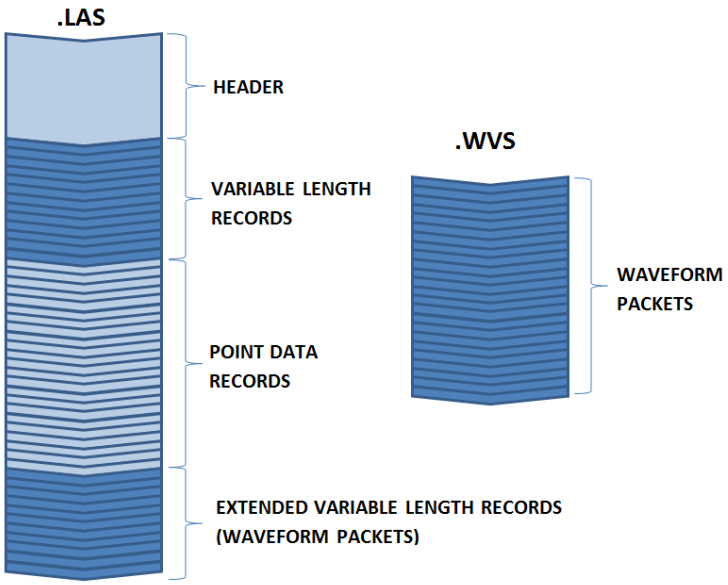

Figure 2-3

2.3 Leica Vs Trimble Instruments: Limitations, Differences and Advantages

As shown in Figure 2-1, the Leica ALS 50-II instrument was used to capture the LiDAR data of New Forest dataset and the Trimble AX60 for collecting the RedGum Forest FW LiDAR data. It is therefore important to clarify the differences, the limitations and the advantages of each instrument.

The Trimble performs at frequency 400kHz, while the Leica's maximum scanning frequency is 120kHz. Nevertheless, during experiments there were occasions when the

Leica discarded every other waveform by exceeding its maximum scanning frequency [19]. The New Forest dataset has been affected with this bug and on average 34.9(this is for one file I need to do it for the entire dataset)***% of the saved pulses only contain discrete data. We should therefore be extremely careful when comparing Discrete with FW LiDAR data. At [20], it is stated that extra information, the echo-width, from the FW LiDAR data are relatively unimportant but the New Forest datasets were used for the comparison and there is no mention about the significantly less waveforms recorded in comparison to the discrete data.

Another problem with the Leica sysyem is the small range of intensities due to the number of bits used for recording them; the Leica system uses 8bits integers (0-255 range) while the Trimble uses 2bits integers (0-16385 range). For increased range and finer intensities, the Automatic Gain Controller (AGC) value was introduced. The AGC is an 8bit number that defines how the recorded intensity range is shifted across a wider range of intensities. The AGC value is adjusted according to the reflected laser intensity of the previous pulse and it therefore varies across a flightline. Consequently, the raw intensities are incomparable to each other and since the relation between AGC and the intensities is not linear, the range normalisation is complicated [21] [22]. In this thesis, the intensities of the Leica system are used as boolean values (whether something exist or not using a user-defined threshold) to quickly overcome that issue and focus on the major research objectives. Regarding the Trimble instrument, there is no AGC value because the intensities are saved into a 16bit integer and as long as the flight height is constant no normalisation is required. In a few words, the raw intensities recorded using the Leica system are not normalised and therefore not comparable to each other, while the intensities of the Trimble instrument are more meaningful.

Moreover the footprints of the laser on the ground depends on the scanning pattern of the instruments and the field of view. The sinusoidal scanning pattern of Leica system results into higher intensity of footprints at the edges of the flightline. The footprints of the Trimble instruments are more equally spaced because they are scanned using a rotating polygon. The problem of the uneven footprints of the Leica system is solved by normalisation during the voxelisation but the equally spaced footprints are more prone to aliasing when voxelised. Regarding the field of view, Leica has a wider field of view but in both cases big angles are avoided because otherwise data look deformed at edges of the flightlines.

Last but not least, the sensor of the Trimble instrument is a native full-waveform sensors and the discrete LiDAR are produced by extracting peak points at post-processing. Therefore the concept of extracting a denser point clouds using Gaussian decomposition [13] does not apply on data collected with those sensors. That was also proved

by extracting peak points from Trimble FW LiDAR data using the pulseextract from LAStools [23]; the number of points extracted was exactly the same as the number of points saved into the associated discrete LiDAR files. Therefore Discrete data from the Trimble instrument are the same as FW LiDAR point cloud generated by echo decomposition and peak points extraction.

To sum up, the Trimble AX60 instrument is a newer sensor and therefore has less problems in comparison to the Leica ALS50-II instrument. Table **??** summarises the differences between the two sensors.

Instrument Name:	**Leica ALS550-II**	**Trimble Ax60**
Scanned Area	New Forest, UK	RedGum, Australia
Year of Introduction:	Discrete LiDAR 2009 & FW LiDAR 2010	2013
Max Scan Frequency (kHz):	120	400
Recorded Intensity (bits):	8	16
AGC:	Yes	No
Scanning Pattern:	Sinusoidal	The footprints are more equally spaced on the ground
Max field of view (degrees):	75	60

Table 2.1: Specifications of the LiDAR instruments used

2.4 Hyperspectral Imagery

Hyperspectral imagery has a positive impact in remote sensing because they contain information beyond human's visibility. The human eye receives light from the visual spectrum into three bands (red, green and blue). The hyperspectral sensors captures a larger spectrum and divides its light components into hundreds of bands, recording this way more information than a human eye can receive [12].

Nevertheless, raw airborne images appear deformed because the pixel length varies across the flightline. NERC ARSF geo-corrects the data using the Airborne Processing Library (APL) [24]. The processing levels are numbered. At 'level 3' the pixels are equally spaced and sized, but are slightly blurred. In this thesis, the 'level 1' data are used to preserve the highest possible quality. The 'level 1' data are non geo-corrected but they are associated with a file that defines the spatial location of each pixel. In practise, there are two files, the '.bil' and the '.igm'. The '.bil' file contains the hyperpsectral cube (Figure 2-4), all the pixel values at different wavelengths, and the .igm file gives the x, y, z coordinates of each pixel.

The number of bands and the spectrum range captured depends on the hyperspectral sensor. The data from New Forest were collected using the following instruments:

- the Eagle, which captures the visible and near infra-red spectrum (400-970nm)
- the Haw, which covers short wave infra-red wavelengths(970-2450nm)

Both sensors divide their spectrum range into 252 bands and each band is a 2D vector as shown in Figure 2-4).

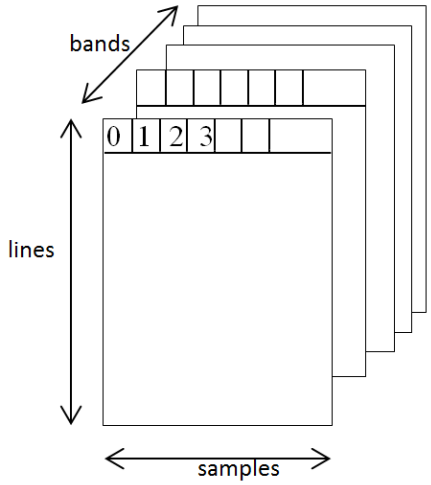

Figure 2-4: This figure shows the order of the hyperspectral pixels saved into the the binary .bil file.

By the way, the hyperpsectral images also come with a number of drawbacks. A few are mentioned here but since hyperpsectral imagery is not the main focused of the thesis there are not addressed:

- System faults sometimes occurs and the affected areas are masked out. This results into blank areas.
- As a passive sensor, it is weather dependant and some areas are covered with clouds.
- Due to the high refraction of light at some wavelength, some bands are highly influenced by humidity (i.e. wavelength 1898.33).

To sum up, hyperpsectral images contain information beyond the visible and they are delivered into two file, one contains the hyperspectral cube and the other one the geo-locations of each pixel. In this project, they are used at chapter (Chapter 6), where it is shown that the combination of Remote Sensing data confers better results for generating tree coverage maps.

Chapter 3

Pipeline

3.1 Overview of Thesis

This research aims to ease the way of handling full-waveform (FW) LiDAR data for remote forest surveys. The primary output of this thesis is the open source software DASOS (=forest in Greek), which aims to break the barrier between understanding and using the FW LiDAR (for more information about DASOS please refer to Section 3.3). New representations of the FW LiDAR are further proposed for handling the data. The contributions of DASOS and the new representations of the FW LiDAR are demonstrated in three applications:

- Visualisations and optimisations on managing real volumetric data:
- Alignment with hyperspectral images for generating tree coverage maps:
- Dead Tree detection for managing biodiversity in Australian native forests:

3.2 Objectives

The overarching aim of future work is to improve and optimise visualisations of full-waveform LiDAR data and hyperspectral images for remote forest surveying.

Objectives:

1. Enable browsing of very large scale datasets with many points and spectral bands in an efficient manner 2. Estimate tree coverage and investigate the potential of integrating multiple remote sensing datasets in forestry 3. Tree crown detection and height estimations in comparison to human detection, which will benefits wood trade and forest management 4. Enable experts to establish wood coverage 5. Enable understanding

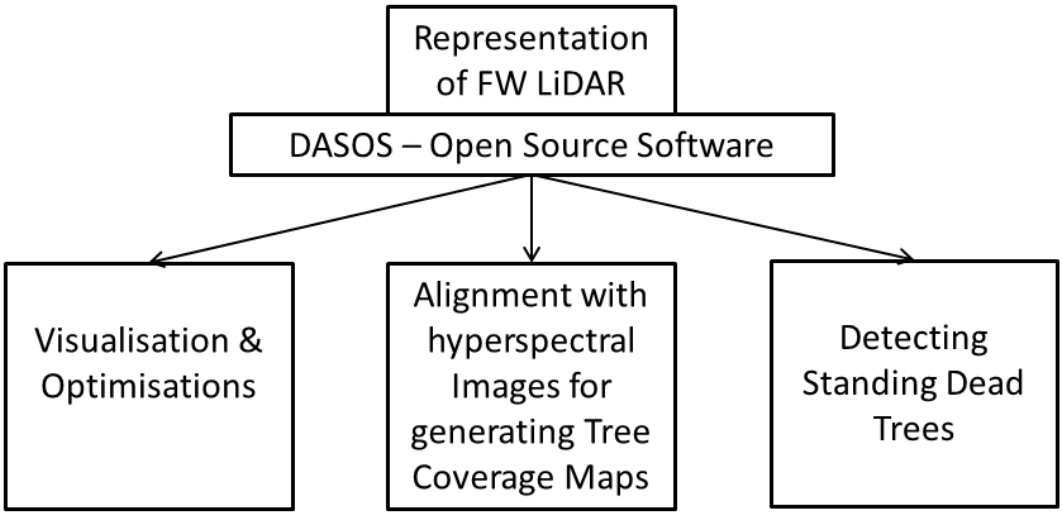

Figure 3-1: The pipeline of the thesis

of forestry concepts through 3D visualisations 6. Investigate data structures that will be better for volumetric rendering and efficient management of large point clouds

This project explores visualisation and data-understanding for full waveform LIDAR systems.

- How can large full waveform datasets be effectively and efficiently visualised? (especially in combination with other forms of data, such as hyperspectral images). - How can terrain classification systems can be modified to effectively make use of full-waveform data? (for example, detection of dead trees for protecting animals living inside dead trees in Australia). - Can visualisation and classification be improved by inference of high quality 3D information, for example, using priors over the space of 3D elements and compatibility between multiple observations? The project will also encompass other facets of large volume environmental dataset visualisation and understanding as appropriate.

3.3 DASOS

DASOS can produce 3D polygons and metrics useful in deriving information about the scanned areas

Chapter 4

Voxelisation of FW LiDAR data

4.1 Background Information

*** the following paragraphs were moved here from the Background Chapter 1.2 and the blue text was added

The most common approach of interpreting the FW LiDAR is the Gaussian decomposition of the waveforms and extraction of peak points [25]. Neunschwander et al used this approach for Landcover classification while Reitberger et al applied it for distinguishing deciduous trees from coniferous trees [26] [27]. Chauve et al further proposed an approach of improving the Gaussian model in order to increase the density of the points extracted from the data and consequently improve point based classifications applied on FW LiDAR data [17].

While echo decomposition identifies significant features as points, the FW LiDAR data also contains information in single shots that may be below the significance threshold. The waveform samples data can be accumulated from multiple shots into into a voxel array, building up a 3D density volume. The correlation between multiple pulses into a voxel representation produces a more accurate representation, which confers greater noise resistance and it further opens up possibilities of vertical interpretation of the data. Voxelisation was firstly introduced by Persson et al, who used voxelisation to visualise the waveforms using different transparencies [28] and it seems to be the future of FW LiDAR data with the literature to moving toward that direction. In 2016, Cao et al used it for tree species identification [29] and Sunmall et al characterised forest canopy from a voxelised vertical profile [20]. This innovative approach is an integral part of this thesis and it is used for both visualisations and classifications [30] [31].

*** end of moved paragraphs ***

4.2 3D Discrete Density Volume

Similar to Person et al, the waveforms are converted into voxels by inserting the waves into a 3D discrete density volume. But in this approach the noise is removed by a threshold first. When a pulse doesn't hit any objects, the system captures low signals which are noise. For that reason, the samples with amplitude lower than the noise level are discarded. Further, to overcome the uneven number of samples per voxel, the average amplitude of the samples that lie inside each voxel is taken, instead of selecting the sample with the highest amplitude [28]:

$$I_v = \frac{\sum_{i=1}^{n} I_i}{n} \tag{4.1}$$

Where n = number of samples of a voxel, Ii = the intensity of the sample i, Iv is the accumulated intensity of the voxel. The main issue of that approach is that the intensities of the LiDAR data haven't been calibrated. Non calibrated intensities do not significantly affect the creation of polygon meshes, because during polygonisation, the system treats the intensities as Booleans; is that voxel empty or not? Nevertheless, the noise level could be set lower if the intensities were calibrated and more details would be preserved on the polygon meshes. For that reason, calibrating the intensities of the return is a task needing to be performed in order to enable the use of intensities in future classifications.

4.3 Implicit Object

Once the 3D discrete density volume is generated, numerical implicitization of objects is used to represent the scanned area. Numerical implicitization was introduced by Blinn in 1982 [32]. A function $f(X)$ defines an object, when for every n-dimensional point X that lies on the surface of the object, satisfied the condition$X = \alpha$. Numerical implicitization enables definition of complex object without saving large amounts of triangles.

The 3D volume, generated as explained in the previous section, is used as a discrete density function $f(X), \alpha$ to represent an object (Pasko and Savchenko, 1994):

f(X) = α , when X lies on the surface of the object

f(X) > α , when X lies inside the object and

f(X) < α , when X lies outside the object

where

X = a 3D point (x, y, z) representing the longitude, latitude and height respectively

f(X) =the discrete density function that takes X as input and returns the accumulated

intensity value of the voxel that X lies in
α = the isolevel of the object and defines the boundary of the object.
f(X) is equal to α iff X lies on the surface of the object. The isolevel α is a user defined parameter and varies depending on the amount of noise in the data.

4.4 Normalisation

- Normalisation: each sample intensity represents the amount of radiation return into a constant time interval. Therefore to normalise the intensities across the voxels the average of the number of samples added to the voxels is taken. Example if 5 samples are inside a voxels and the waveform is digitised at 2ns, therefore 10ns internal of waveform is saved into that voxels. To keep it consistent the length of waveform across the voxels the average intensity of the number of samples inserted into each voxel is taken.

4.5 Integral Volumes

In 1984, Crow proposed an image representation where each pixel value is replaced by the sum of all the pixels that belong to the rectangle defined by the lower left corner of the image and the pixel of our interest (Crow, 1984). Even though more storage space is required to save the image, due to the larger numbers, the sum of every rectangle in the image can be calculated in constant time, once the table is constructed. The integral image can also be constructed in linear time O(n), where n is the number of pixels in the image. One iteration through the entire image is enough to replace the pixel values of the image.

image

Chapter 5

Visualisations

Even though numerical implicitization is beneficial in reducing storage memory and for various resolution renderings of the same object, visualising numerical/algebraic objects is not straight forward, since they contain no discrete values. More information about visualisations are given at Section 5.

A big part of this thesis is the way of handing data and how algorithmic approaches can speed up accessing of FW LiDAR data while keeping memory allocation low. The next sections explains the data structures implemented and the new ones proposed during this studies. The functionalities are explained here while their performance is discussed at section 5.

The names of the data structures are the given below. Some names are from standard data structures and the new ones proposed have

1. 1D array
2. 1D hashed array
3. Octree
4. Integral Volumes
5. Integral Tree
6. Hashed OCtree
7. Series of Hashed Octrees

Even though numerical implicitisation is beneficial in reducing storage memory and for various resolution renderings of the same object, visualising numerical/algebraic objects is not straight forward, since they contain no discrete values. This problem can either be address either by ray-tracing or polygonisation. In 1983, Hanraham suggested a ray-tracing approach, where an equation is derived from the ray and surface intersection [33]. The Marching Cubes algorithm was later introduced for polygonising implicit objects. The algorithm first divides the space into cube and then creates consistent

triangle using look up table [34].

The Marching cubes algorithm constructs surfaces from implicit objects using a search table. Let's assume that f(X) defines an implicit object. At first the space is divided into cubes, named voxels. Each voxel is defined by eight corner points, which lie either inside or outside the object. By enumerating all the possible cases and linearly interpolating the intersections along the edges, the surface of the implicit object is constructed [34].

According to Lorensen and Cline, the normal of each vertex is calculated by measuring the gradient change. But in our case, due to the high gradient changes inside the volume, calculating the normal in that way leads to a non-smooth visualisation. For that reason, in this research the normal of each vertex is equal to the average normal of its adjacent triangles.

Further the sampling of the Marching cubes is independent from the sampling of the 3D density volume. Therefore consistency between the two is required and more information about that is given at the results section 4.5.5.

5.0.1 Optimising Marching Cubes

The original Marching Cubes algorithm uses a scan line approach and processes all the cubes sequentially. The scan line approach sometimes implies looping through large amounts of empty cubes. To optimise the process, in this research, it is proposed an algorithm that repeatedly divides the volume and utilities Integral Volumes to discard empty volumes during the polygonisation. Using this optimisation algorithm it was achieved an up to 51This optimisation algorithm is explained in the following sections, which are structured as follow: - Background information, including previous related work. - How integral images are extended into 3D. - The proposed algorithm of using Integral Volumes to speed up the process of polygonising an implicit object using the Marching Cubes algorithm - Implementation details that contribute to the efficiency and speed up of the algorithm - Results

5.0.2 Background

Much research has been done so far on optimising and improving the polygonisation of implicit surfaces. But most research is based on closed and manifold object. A polygon mesh is closed when it has no holes and it is manifold when it can be unfolded into a 2D continues surface. In order to guarantee consistent topology, an optimised approach with an enhanced look up table was proposed by Lewiner et al in 2003.

Further surface-tracking was discussed in both papers of (Rodrigues de Araujo and Pires Jorge, 2005) (Hartmann, 1998). Starting from a seed point, the surface is expanded according to the local curvature of the implicit object. Self-intersections and collisions are avoided using heuristic edge length. This method is considered to be faster and more efficient, in comparison with the Marching Cubes algorithm. Because, by tracking the surface, huge empty spaces are not searched and it is also possible to create smaller triangles on places with high gradient changes and bigger triangles on surfaces with low variance. Nevertheless, surface-tracking Algorithms cannot be applied in our case though, because the output of on my program is a non-manifold objects. The 3D Volume generated from FW LiDAR data is not consistent, since small footprint Leica FW systems cannot guarantee that the last return is from the ground. For that reason, it is possible that some trees may be separated from the ground. Surface-tracking algorithms converge once the object is closed. Therefore, there is a possibility that they may converge after polygonising a single tree if the seed point lies on a tree that is separated from the ground.

In 1992, Hansen and Hinker proposed parallelising the polygonisation process of BlobTree trees on Single Instruction, Multiple Data (SIMD) machines. BlobTree trees represent implicit objects as a combination of primitives and operations likes union and blends (Galbraith, MacMurchy, and Wyvill, 2004). While the depth of the tree increases, the time required to get the value that defines whether a point is inside or outside the object increases as well. On SIMD machines greater speed up is achieved at longer instruction due to the less communication cost. Therefore parallelising the process of BlobTree trees with long depth is beneficial, but in our case the value returned for a given point is calculated in constant time. Further, according to the C++ Coding Standards by Sutter and Alexandrescu, when optimisation is required is better to seek an algorithmic approach first because it is simpler to maintain and the possibility of being bug free is higher (Sutter and Alexandrescu, 2004).

OpenVDB library manages volumetric data with octrees. My program uses 1D ar-

rays allowing constant time access of voxel values and by importing OpenVDB library, its speed was significantly decreased; while the number of voxels is increasing the time required to get the value of a voxel is also increasing. Further according to the documentation, the VolumeToMesh class "meshes any scalar grid that has a continuous isosurface", while the surface of the FW LiDAR volumes is not continuous; there are triangles that represent leafs inside the trees and some of the trees may be disconnected from the ground because the last return do not always reach the earth (OpenVDB 2.3.0).

In this report, it is introduced a new method of optimising the marching cubes algorithm. This method utilises Integral Volumes (an extension of Integral Images) to discard chunks of empty cubes during polygonisation. Its effectiveness stands at the ability of integral volumes to find the sum of any sub-volume into constant time and it is important because it works effectively non-manifold or non-closed objects.

Chapter 6

Alignment with Hyperspectral Imagery

6.1 Classifications

This talk presents the new features of DASOS, which is an open source software for managing full-waveform LiDAR data and those features are used for detecting dead standing Eucalypt.

The value of dead standing Eucalypt trees from a biodiversity management perspective is large. In Australia, many arboreal mammals and birds that are close to extinct inhabit hollows [5]. Nevertheless, studies predict shortage of hollows in the near future due to tree harvesting and the decades required for a tree to be mature enough to develop a hollow [3] [4]. Dead standing eucalypt trees are more likely to be aged and have hollows, therefore automated detection of them plays a significant role in protecting animals that rely on hollows.

DASOS (= $\delta\acute{\alpha}\sigma o\varsigma$) means forest in Greek and it is an open source software aiming to ease the way of handling FW LiDAR data in forestry [31]. Traditional ways of interpreting FW LiDAR data, suggests extraction of a denser points cloud using Gaussian decomposition [26] [27]. Nevertheless DASOS was influenced by Persson et al, 2005, who used voxelisation to visualise the waveforms [28]. But, DASOS do not only uses voxelisation for visualisations but also for extracting metrics useful in classification. It further normalises the intensities so that equal pulse length exists inside each voxel, making intensities more meaningful. It is further seems that the literature is moving towards voxelisation with the good results obtained at recent publication on tree species classification [29].

The new features of DASOS: New features of DASOS which enables observation at tree level: i.e. distribution of intensities at specific area

The data, provided by RPS Australia East Pty Ltd, were collected in March 2015 from the Riegl (LMS-Q780 or LMS-Q680i?) sensor at an Australian native Forest with eucalyptus. The fieldplots has been provided by (Interprine Group Ltd or Forest Corporation?).

examined with Random Forest

The new features of DASOS are presented and used for generating 3D signatures characterising dead standing trees and a comparison between the discrete and FW LiDAR data is performed to demonstrate the increased survey accuracy obtained with the FW LiDAR.

This paper presents a new feature of DASOS, which is an open source software for managing full-waveform (FW) LiDAR data and that feature is used for detecting dead standing Eucalypt trees in native Australian forests.

The value of dead standing Eucalypt trees from a biodiversity management perspec-

tive is large. In Australia, many arboreal mammals and birds, which are close to extinct, inhabit hollows [5]. Nevertheless, studies predict shortage of hollows in the near future due to tree harvesting and the decades required for a tree to develop a hollow [3] [4]. Dead standing eucalypt trees are more likely to be aged and have hollows, therefore automated detection of them plays a significant role in protecting animals that rely on hollows.

The LiDAR data used for this project are provided by RPS Australia East Pty Ltd and they were collected in March 2015 using the Riegl (LMS-Q780 or LMS-Q680i?) sensor. The Riegl LMS-Q??? is a native full-waveform sensor and the LiDAR point clouds were generated from the waveform instrument data during post processing. In addition, the field plots used for the classifications are provided by (Interprine Group Ltd or Forest Corporation?) and contain around 1000 Eucalypt trees while 10% of them are dead.

The new feature of DASOS calculates forestry metrics within a radius relevant to canopy height and exports all metrics into a single vector for fast interpretation in advanced statistical tools. Traditional ways of interpreting FW LiDAR data, suggests extraction of a denser points cloud [26] [27], but as mentioned before with the Riegl system this is done at post processing. Nevertheless DASOS was influenced by Persson et al, 2005, who used voxelisation to visualise the waveforms [28], but DASOS also uses it for generating metrics. It further normalises the intensities so that equal pulse length exists inside each voxel, making intensities more meaningful. Further, recent publication on tree species classification showed that voxelisation could confer good results while interpreting FW LiDAR data [29].

Previous work on dead standing trees detection, suggests single tree segmentation before dead trees identification [35] [36] but in case of Eucalypt trees single tree detection is a challenge on its own due to their irregular structure and multiple trunk splits.

In this project, the new feature of DASOS is used for generating 3D signatures characterising dead standing Eucalypt trees and a comparison between the LiDAR point cloud and FW LiDAR data is performed using Random Forest to demonstrate the increased survey accuracy obtained with voxelisation.

Chapter 7

Overall Results

Chapter 8

Conclusions

8.1 Contributions

Bibliography

[1] T. Elmqvist, C. Folke, M. Nyström, G. Peterson, J. Bengtsson, B. Walker, and J. Norberg, "Response diversity, ecosystem change, and resilience," *Frontiers in Ecology and the Environment*, vol. 1, no. 9, pp. 488–494, 2003.

[2] D. U. Hooper, F. S. Chapin Iii, J. J. Ewel, A. Hector, P. Inchausti, S. Lavorel, and B. Schmid, "Effects of biodiversity on ecosystem functioning: a consensus of current knowledge," *Ecological monographs*, vol. 75, no. 1, pp. 3–35, 2005.

[3] D. B. Lindenmayer and J. T. Wood, "Long-term patterns in the decay, collapse, and abundance of trees with hollows in the mountain ash (eucalyptus regnans) forests of victoria, southeastern australia," *Canadian Journal of Forest Research*, vol. 40, no. 1, pp. 48–54, 2010.

[4] R. L. Goldingay, "Characteristics of tree hollows used by australian birds and bats," *Wildlife Research*, vol. 36, no. 5, pp. 394–409, 2009.

[5] P. Gibbons and D. Lindenmayer, *Tree Hollows and Wildlife Conservation in Australia*. CSIRO Publishing, 2002.

[6] "Animal pests: Poss."

[7] D. H. DeHayes, P. G. Schaberg, G. J. Hawley, and G. R. Strimbeck, "Acid rain impacts on calcium nutrition and forest health alteration of membrane-associated calcium leads to membrane destabilization and foliar injury in red spruce," *BioScience*, vol. 49, no. 10, pp. 789–800, 1999.

[8] J. Holmgren, "Prediction of tree height, basal area and stem volume in forest stands using airborne laser scanningce," *Scandinavian Journal of Forest Researcht*, vol. 19, no. 6, pp. 543–553, 2004.

[9] S. G. Aracil and R. B. A. Herries, D.L, "Evaluation of an additional lidar metric in forest inventory," *Proceedings of Silvilaser*, 2015.

[10] M. J. Harper, M. A. McCarthy, R. Van Der Ree, and J. C. Fox, "Overcoming bias in ground-based surveys of hollow-bearing trees using double-sampling," *Forest Ecology and Management*, vol. 190, no. 2, pp. 291–300, 2004.

[11] L. Rayner, M. Ellis, and J. E. Taylor, "Double sampling to assess the accuracy of ground-based surveys of tree hollows in eucalypt woodlands," *Forest Ecology and Management*, vol. 36, no. 3, pp. 252–260, 2011.

[12] R. B. Smith, *Introduction to Hyperspectral Imaging*. MicroImages, 2014.

[13] W. Wanger, A. Ullrich, T. Melzer, C. Briese, and K. Kraus, "From single-pulse to ful-waveform airborne laser scanners," *ISPRS Journal of Photogrammetry and Remote Sensing*, vol. 60, pp. 100–112, 2004.

[14] A. Wehr and U. Lohr, "Airborne laser scanning - an introduction and overview," *ISPRS Journal of Photogrammerty and Remote Sensing*, vol. 54, pp. 68–82, 1999.

[15] C. Mallet and F. Bretar, "Full-waveform topographic lidar: State-of-the-art," *ISPRS Journal of Photogrametry and Remote Sensing*, vol. 64, pp. 1–16, 2009.

[16] K. Anderson, S. Hancock, M. Disney, and K. Gaston, "Is waveform worth it? a comparison of lidar approaches for vegetation and landscape characterization," *Remote Sensing in Ecology and Conservation*, 2015.

[17] A. Chauve, C. Mallet, F. Bretar, S. Durrieu, M. Deseilligny, and W. Puech, "Processing full-waveform lidar data: Modelling raw signals," *International Archives of Photogrammetry, Remote Sensing and Spatial Information Sciences*, 2007.

[18] *LAS Specification version 1.3-R1*. Bethesda, Maryland: American Society for Photogrammetry and Remote Sensing, 2010.

[19] M. Warren, *Full Waveform Upgrade*. NERC ARSF wiki, 2012.

[20] M. J. Sumnall, R. A. Hill, and S. A. Hinsley, "Comparison of small-footprint discrete return and full waveform airborne lidar data for estimating multiple forest variables," *Remote Sensing of Environment*, vol. 173, pp. 214–223, 2016.

[21] K. H. R. A. . Z. A. Lehner, H., "Consideration of laser pulse fluctuations and automatic gain control in radiometric calibration of airborne laser scanning data.," *Proceedings of 6th ISPRS Student Consortium and WG VI/5 Summer School*, 2011.

[22] I. Korpela, H. O. Ørka, H. V. Hyyppä, J., and T. Tokola, "Range and agc normalization in airborne discrete-return lidar intensity data for forest canopies," vol. 65, no. 4, pp. 369–379, 2010.

[23] M. Isenburg, *LAStools - efficient tools for LiDAR processing.* rapidlasso.

[24] M. Warren, B. Taylor, M. Grant, and J. D. Shutler, "Data processing of remorely sensed airborne hyperspectral data using the airborne processing library (apl)," *ScienceDirect, Computers and Geosciences*, vol. 64, 2014.

[25] W. Wanger, A. Ullrich, V. Ducic, T. Maizer, and N. Studnicka, "Gaussian decompositions and calibration of a novel small-footprint full-waveform digitising airborne laser scanner," *ISPRS Journal of Photogrammetry and Remote Sensing*, vol. 60, pp. 100–112, 2006.

[26] A. Neuenschwander, L. Magruder, and M. Tyler, "Landcover classification of small-footprint full-waveform lidar data," *Jounal of Applied Remote Sensing*, vol. 3, no. 1, pp. 033544–033544.

[27] J. Reitberger, P. Krzystek, and U. Stilla, "Analysis of full waveform LiDAR data for tree species classification," *International Journal of Remote Sensing*, vol. 29, no. 5, pp. 1407–1431, 2008.

[28] A. Persson, U. Soderman, J. Topel, and S. Ahlberg, *Visualisation and Analysis of full-waveform airborne laser scanner data.* V/3 Workshop, Laser scanning 2005, 2005.

[29] L. Cao, N. Coops, L. Innes, J. Dai, and H. Ruan, "Tree species classification in subtropical forests using small-footprint full-waveform lidar data," *International Journal of Applied Earth Observation and Geoinformation*, vol. 49, pp. 39–51, 2016.

[30] M. Miltiadou, M. Grant, M. Brown, M. Warren, and E. Carolan, "Reconstruction of a 3d polygon representation from full-wavefrom lidar data," *RSPSoc Annual Conference 2014, New Sensors for a Changing World*, 2014.

[31] M. Miltiadou, M. A. Warren, M. Grant, and M. Brown, "Alignment of hyperspectral imagery and full-waveform lidar data for visualisation and classification purposes," *The International Archives of Photogrammetry, Remote Sensing and Spatial Information Sciences*, vol. 40, no. 7, p. 1257, 2015.

[32] J. F. Blinn, *A Generalization of Algebraic Surface Drawing*, vol. 1. ACM Transactions on Graphics (TOG).

[33] P. Hanrahan, "Ray tracing algebraic surfaces," *ACM SIGGRAPH Computer Graphics*, vol. 17, no. 3., 1983.

[34] W. E. Lorensen and H. E. Cline, "Marching cubes: A high resolution 3d surface construction algorithm," *ACM Siggraph Computer Graphics*, vol. 21, pp. 163–169, 1987.

[35] W. Yao, P. Krzystek, and M. Heurich, "Identifying standing dead trees in forest areas based on 3d single tree detection from full-waveform lidar data," *ISPRS Annals of the Photogrammetry, Remote Sensing and Spatial Information Sciences*, vol. I-7, pp. 359–364, 2012.

[36] P. Polewski, W. Yao, M. Heurich, P. Krzystek, and U. Stilla, "Active learning approach to detecting standing dead trees from als point clouds combined with aerial infrared imagery," *Proceedings of the IEEE Conference on Computer Vision and Pattern Recognition Workshops*, pp. 10–18, 2015.

Chapter 9

Appendices

9.1 Birds and Mammals Catalogue

9.1.0.1 Introduction

9.1.0.2 Australian arboreal Mammals

9.1.0.3 Australian Birds

The Forestry Corporation, Australia, provided a list of bird species that rely on hollows. But species are not limited to that list and more species rely uses hollows for shelters.

The provided list of the birds is divided into three groups:

1. Categorised as threatened species according to the Environement Protection and Biodiversity Conservation Act, 1999

Corella Eastern Rosella Superb Parrot Barking Owl Masked Owl

2. All the above species are included to the Action Plan for Australian Birds, 2000, as well as the following once:

Powerful Owl Sooty Owl

3. The rest:

Kookaburra Sulphur Crested Cockatoo Crimson Rosella Rainbow Lorikeet Musk Lorikeet Little Lorikeet Red-winged Parrot Cockatiel Australian Ringneck (Parrot) Red-rumped Parrot Powerful Owl Sooty Owl Barn Owl White-throated Treecreeper

9.1.0.4 Web-links of Photos

Mammals · Brush-tailed Possum - protected wildlife (Hollow: http://www.cavershamwildlife.com.au/comm brushtail-possum/) (`http://www.rymich.com/girraween/photos/animals/mammals/possums/trichosu`

Birds · Kookaburra (`http://tenrandomfacts.com/blue-winged-kookaburra/`) · Sulphur Crested Cockatoo (`http://aussiegal7.deviantart.com/art/Sulphur-Crested-Cockatoo-08-`

· Corella (http://www.theparrotplace.co.nz/all-about-parrots/long-billed-corella/) · Crimson Rosella (http://25.media.tumblr.com/tumblr_m3mo89c40r1r4t9h1o1_1280.jpg) · Eastern Rosella (http://2.bp.blogspot.com/-pYxw51WjSOY/UB-LEFgd2KI/AAAAAAAAAWg/9z60PUWE6TE/s1600/_GJS6601-as-Smart-Object-1.jpg) · Galah (https://www.pinterest.com/pin/537546905498955709/) · Rainbow Lorikeet (https://www.reddit.com/r/pics/comments/328fvc/a_rainbow_lorikeet_found_in_coastal_regions/) · Musk Lorikeet ((http://www.rymich.com/girraween/photos/animals/birds/medium/glossopsitta_concinna/glossopsitta_concinna_001.jpg) · Little Lorikeet (http://www.pbase.com/sjmurray/psittacidae) · Red-winged Parrot (https://www.pinterest.com/pin/395894623469889727/) · Superb Parrot (http://www.davidkphotography.com/?showimage=637) · Cockatiel (http://up.parsipet.ir/uploads/Cockatiels-for-sale.jpg) · Australian Ringneck (Parrot) (http://ontheroadmagazine.com.au/wp-content/uploads/2015/09/Twenty-eight-parrot-2jpg) · Red-rumped Parrot (http://parrotfacts.net/wp-content/uploads/Red-Rumped-Parrot-on-a-jpg) · Powerful Owl (http://farm1.staticflickr.com/219/495796536_f78dac04c1.jpg) · Sooty Owl (hollow: http://www.mariewinn.com/marieblog/uploaded_images/screech2-738532.jpg) (http://www.owlpages.com/owls/species/images/greater_sooty_owl_richard_jackson-1.jpg) · Barking Owl (http://www.pcpimages.com/Nature-and-Wildlife-Birds/i-7JKSTp5/1/L/owl%20%281%20of%201%29-L.jpg) · Masked Owl (http://www.survival.org.au/images/birds/masked_owl_2_600.jpg) · Barn Owl (Hollow: http://www.barnowltrust.org.uk/wp-content/uploads/Barn_Owl_hollow_tree-wallpaper.jpg) (https://upload.wikimedia.org/wikipedia/commons/c/c6/Tyto_alba_-British_Wildlife_Centre,_Surrey,_England-8a_%281%29.jpg)

· White-throated Treecreeper (http://www.birdlifemelbourne.org.au/bird-lists/47-Treecreepers/White-throated-Treecreeper/White-throated%20Treecreeper%202%20JB.jpg) (hollow: https://geoffpark.files.wordpress.com/2011/09/female-white-throated-tre jpg)

Hollow Owl : http://www.mariewinn.com/marieblog/uploaded_images/screech2-738532.jpg